

# Investigation of Cation Distribution and Microstructure of Nano Ferrites Prepared by Different Wet Methods

Ebtesam Ateia<sup>1</sup> · Lobna M. Salah<sup>1</sup> · Asmaa A. H. El-Bassuony<sup>1</sup>

Received: 25 March 2015 / Accepted: 8 June 2015 / Published online: 3 July 2015  
© Springer Science+Business Media New York 2015

**Abstract** Nanostructure ferrite of composition  $\text{Ni}_{0.5}\text{Zn}_{0.5}\text{Cr}_{0.1}\text{Fe}_{1.9}\text{O}_4$  was prepared by sol–gel, co-precipitation, citrate-gel, flash and oxalate precursor methods. Structural and micro structural analysis of the investigated samples were carried out by X-rays diffractometer (XRD), infrared spectroscopy, transmission electron microscopy (TEM) and atomic force microscope. It was observed that the lattice parameter of cubic spinel was constant, and the positions of both tetrahedral and the octahedral bands had the fixed positions for all methods except flash and oxalate precursor methods. These results were explained on the basis of theoretical calculation of cation distribution for Ni–Zn–Cr ferrite. The average crystalline sizes of the investigated samples deduced by TEM were in good agreement with the one estimated by XRD. The above results were correlated to the results of magnetic measurements of the investigated samples.

**Keywords** Ceramics · Chemical synthesis · X-ray scattering · Infrared spectroscopy (IR) · Hysteresis

## 1 Introduction

The synthesis of magnetic nano-particles has been an interesting area of study due to its spread applications [1–5]. Special focus has been placed on obtaining ferrite as

a particulate environment through unconventional methods, especially wet chemical methods [6, 7]. These chemical methods are very promising in terms of the possibility of obtaining a rigorous control of the particle size. But many workers have reported [8–11] that ferrites prepared by wet chemical methods (e.g., co-precipitation) are known to display different cation distribution over the tetrahedral (A) and octahedral (B) sites than ferrites prepared by standard ceramic methods. Hence, both cation distribution and the particle size are very important parameters that play a significant role in determining the magnetic properties of ferrites. So, the aim of the present study is to investigate a familiar composition  $\text{Ni}_{0.5}\text{Zn}_{0.5}\text{Cr}_{0.1}\text{Fe}_{1.9}\text{O}_4$  which has been prepared by different wet chemical methods initiating three major objectives (i) to assess the X-rays diffractometer (XRD) and IR to know the cation distribution (ii) to discuss the relation between crystallite size and magnetic properties (iii) to compare between the different wet chemical methods.

## 2 Experimental Details

### 2.1 Synthesis

The samples under investigation  $\text{Ni}_{0.5}\text{Zn}_{0.5}\text{Cr}_{0.1}\text{Fe}_{1.9}\text{O}_4$  were prepared by various chemical routes, viz. sol–gel, co-precipitation, flash combustion reaction (using two different salts), citrate and oxalate precursor methods. The initial ingredients of metal salt (nitrate, chloride or sulphate) for any method were of high purity (BDH) and were taken in stoichiometric proportion and dissolved each separately in minimum amount of deionized water. The formed cationic solutions were mixed and stirred for half an hour to improve the homogeneity. The resulting solution known as

---

✉ Lobna M. Salah  
Lobna@sci.cu.edu.eg;  
<http://scholar.cu.edu.eg/?q=lobnasalah/>  
Ebtesam Ateia  
ebtesam@sci.cu.edu.eg

<sup>1</sup> Physics Department, Faculty of Science, Cairo University, Giza, Egypt

precursor was used for the following processing techniques [12]:

**Sol–Gel Synthesis** The initial ingredients were nickel nitrate, zinc nitrate, chromium (III) nitrate and iron (III) nitrate. The aqueous solution of polyvinyl alcohol in measured quantities was added drop by drop to the precursor and dehydrated around 100 °C under continuous stirring. Ammonia was added to maintain the suitable pH (between 8 and 9) value. The gelation continued step by step till a slightly red gel type product was formed with the release of reddish brown gas around 100 °C, where the gel was converted into a fluffy ferrite mass which was heated at 400 °C to remove the polyvinyl alcohol.

**Co-precipitation Method** The initial ingredients were nickel chloride, zinc chloride, chromium (III) chloride and iron (III) chloride. The co-precipitating agent, sodium hydroxide aqueous solution, in required quantity was added drop by drop to the precursor under continuous stirring till a massy precipitate was formed. The pH was adjusted to ensure completion of the precipitation. The precipitate was washed with deionized water many times to remove the base and final washing was done with acetone to eliminate water. The filtrate was dried at room temperature to obtain a powder.

**Citrate–Gel Method** The initial ingredients were nickel nitrate, zinc nitrate, chromium (III) nitrate and iron (III) nitrate. The chelating agent, the aqueous solution of citric acid, in measured quantity was added drop by drop to the precursor under constant stirring till a high viscous gel was formed. The ammonia was used to adjust the pH for improving the complication gel. The precursor mixture was then heated at 200 °C to allow evaporation and to obtain a dried product in the form of uniformly colored gray fibers.

**Oxalate Precursor Method** The initial ingredients were nickel sulphate, zinc sulphate, chromium (III) sulphate and iron (III) sulphate. The solution of oxalic acid in measured quantity was prepared using deionized water as solvent and added drop by drop to the precursor under continuous stirring to adjust the pH value at 7. A dense gel was precipitated, which was self burnt at 200 °C to obtain a loose nano powder.

**Flash Combustion Method** In flash the combustion method, two different initial ingredients [nickel, zinc, chromium (III) and iron (III)] of nitrate or chloride salt were used with organic fuel(urea). Urea was added to the weighted mixture of metals salt according to the required stoichiometric proportion 1:6.7 and was well ground. The reactants were hand mixed and heated on a hot plate at 200 °C. At this temperature, the mixture was reacted and gave out gases. The combustion was complete in 3–5 min, and a foamy and highly porous precursor mass was obtained. It was collected and then powdered for further processing.

All the powders prepared from the above five different methods were heated in a furnace at different temperatures and checked by X-ray diffraction to insure the formation of the required chemical formula.

## 2.2 Measurements

The structure and crystallite sizes were tested by XRD using Co-K $\alpha$  radiation ( $\lambda = 1.79026 \text{ \AA}$ ). The nanoparticles average sizes were estimated using Scherrer's relationship [13]. Infrared spectrophotometer study was carried out in KBr medium using Infrared spectrophotometer (Perkin–Elmer 1430) in the range from 200 to 1000  $\text{cm}^{-1}$  with a resolution of 1–5  $\text{cm}^{-1}$ . Morphological and microstructural characterization of the nano ferrites samples were studied by transmission electron microscopy (TEM) JEOL 2010 using model DV 300W1 and scanning probe microscope (SPM-9600) (Shimadzu, Japan). The room temperature magnetic hysteresis of the investigated samples were measured by maximum field 5 kOe using vibrating sample magnetometer (VSM) model 9600-1 LDJ, USA with the hysteresis condition:  $H_{\text{Max}}$ : 4992 Oe and  $H_{\text{Rag}}$ : 10000 Oe.

## 3 Results and Discussion

### 3.1 Structural Analysis

#### 3.1.1 X-ray Analysis

Figure 1 shows XRD pattern for  $\text{Ni}_{0.5}\text{Zn}_{0.5}\text{Cr}_{0.1}\text{Fe}_{1.9}\text{O}_4$  prepared by different wet methods at constant sintering temperature of 200 °C (except co precipitation method prepared at room temperature) for 2 h. The analysis of chart shows that the samples prepared at room temperature and at 200 °C are completely amorphous with appearance of  $\text{Fe}_3\text{O}_4$  as secondary phase. This means that sintering temperature 200 °C is insufficient to form ferrite spinel phase. In other words, the rate of any method is so rapid that cations may not be well distributed to the ferrite lattice.

The complete phase formation of  $\text{Ni}_{0.5}\text{Zn}_{0.5}\text{Cr}_{0.1}\text{Fe}_{1.9}\text{O}_4$  ferrite powders occurred at 600 °C for all different methods except for sol–gel and oxalate methods. For both methods the complete phase formation occurs at 400 and 1000 °C respectively as shown in Fig. 2. The figure shows a single phase cubic spinel structure without any extra lines corresponding to any other phases. All the peaks are matched well with the characteristic reflections of the parent materials as compared with ICDD cards with number (43-0555). Strong diffraction from the planes (220), (311), (400), (511) and (440) as well as a weak diffraction from the planes (222) and (422) are very sensitive to cation distribution at both tetrahedral and octahedral sites. The

**Fig. 1** X-ray powder diffraction pattern for  $\text{Ni}_{0.5}\text{Zn}_{0.5}\text{Cr}_{0.1}\text{Fe}_{1.9}\text{O}_4$  prepared by different wet methods as dried samples

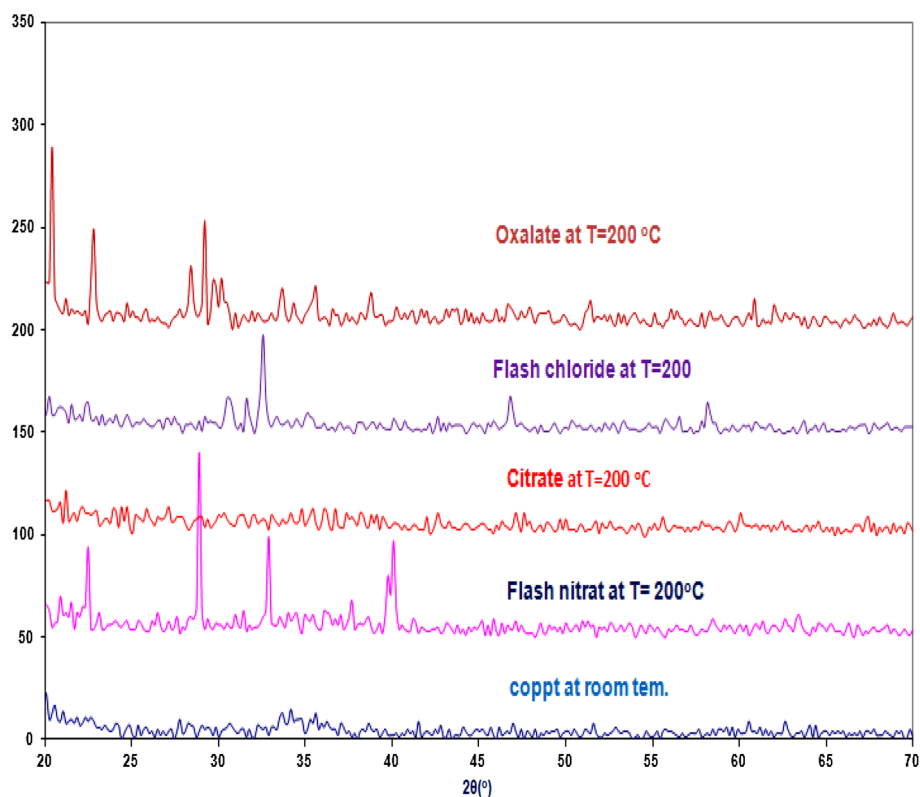
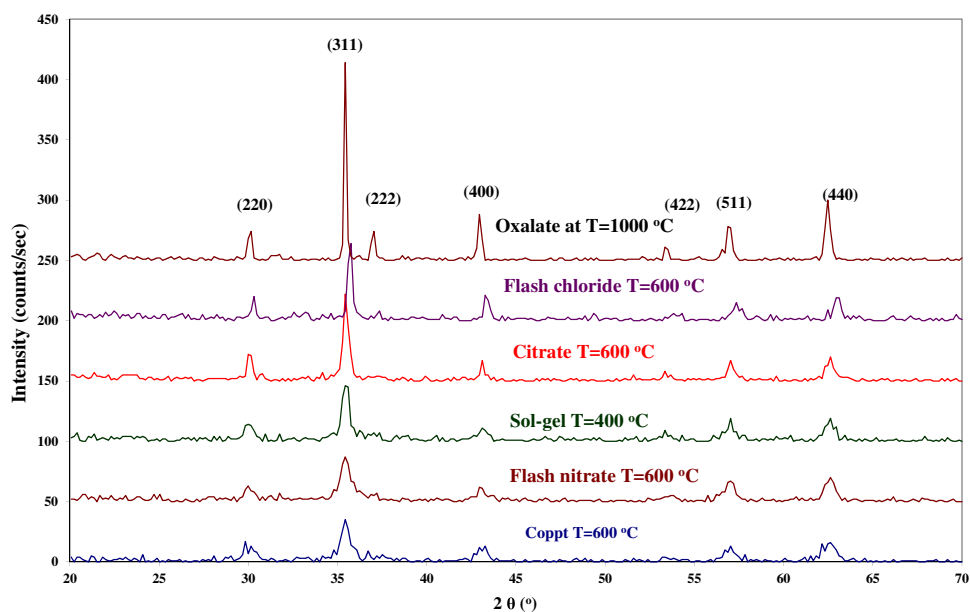


**Fig. 2** X-ray powder diffraction pattern for the samples  $\text{Ni}_{0.5}\text{Zn}_{0.5}\text{Cr}_{0.1}\text{Fe}_{1.9}\text{O}_4$  prepared by different wet methods



(220) plane is occupied by both A and B ions, that is, by Zn, Ni and Fe ions. Consequently the varying cation occupation in both (A) and (B) sites will affect the relative intensity of it [14]. The broadness of peaks indicates ultra fine nature and small crystallite size of particles for all preparation methods except oxalate method. In other words the increase in broadness indicates a decrease of crystallite

size. It is also noticed from the figure that, all the peaks have the same fixed position except two methods. The first is the oxalate precursor method which slightly shifts towards lower  $2\theta$ , while the second is the flash (with chloride salt) method which shifts towards higher  $2\theta$ .

The average values of the calculated lattice parameters from XRD are tabulated in the Table 1. From the Table, it

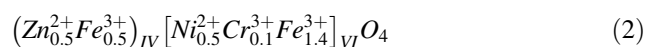
**Table 1** Values of the experimental lattice parameter and estimated crystallite size for  $\text{Ni}_{0.5}\text{Zn}_{0.5}\text{Cr}_{0.1}\text{Fe}_{1.9}\text{O}_4$  prepared by different wet methods

Preparation method	Estimated crystallite size (nm)	Experimental lattice parameter $a_{\text{exp}}$ (Å)
Co-precipitation	16	8.3891
Flash with nitrate salts	18	8.3879
Sol–gel	23	8.3840
Citrate	34	8.3896
Flash with chloride salts	70	8.3347
Oxalate	166	8.4014

is clear that, the lattice parameter is nearly the same except for oxalate precursor and flash (with chloride salt) methods. The theoretical lattice constant  $a_{\text{th}}$  is calculated using the equation [15, 16]:

$$a_{\text{th}} = \frac{8}{3\sqrt{3}} \left[ (r_A + R_0) + \sqrt{3}(r_B + R_0) \right] \quad (1)$$

where  $R_0$  is the radius of the oxygen ion (0.138 nm) [17],  $r_A$  and  $r_B$  are the ionic radii of tetrahedral (A) and octahedral (B) sites respectively. In order to calculate  $r_A$  and  $r_B$ , it is necessary to know the cation distribution for a given system  $\text{NiZnCr}$  ferrite. In general,  $\text{Zn}^{2+}$  ions show a marked preference for the tetrahedral site A where 4s,4p electrons can form covalent bonds with 2p electrons of the oxygen ions [18]. While,  $\text{Ni}^{2+}$  ( $d^8$ ) and  $\text{Cr}^{2+}$  ( $d^3$ ) ions have a tendency to occupy the octahedral site B due to the favourable charge distribution in an octahedral crystal field theory [19]. Generally,  $\text{Fe}^{3+}$  ion has no particular preference for either coordination [20, 21]. Thus, the theoretical cation distribution has to be considered as:



where the brackets ( ) and [ ] indicate A and B sites respectively, so  $r_A$  and  $r_B$  can be calculated for the system by using the following data, the ionic radii for the  $\text{Ni}^{2+}$  (0.69 Å),  $\text{Zn}^{2+}$  (0.60 Å),  $\text{Cr}^{3+}$  (0.62 Å) and  $\text{Fe}^{3+}$  (0.49 and 0.65 Å) depending on its coordination number [22]. Then, the theoretical lattice parameter  $a_{\text{th}}$  is equal to 8.390 Å which is equal the experimental value for all samples except for oxalate and flash (with chloride salt) methods. The insignificance difference between theoretical and experimental lattice parameters confirms both stoichiometric proportion and the theoretical cation distribution given by formula (2). The difference between the theoretical and the experimental lattice parameters for both oxalate and flash methods is attributed to loss of metals ions during synthesis process which will be discussed latter.

The crystallite sizes for all investigated ferrite produced by different methods are calculated using the following Scherrer's equation

$$D = \frac{K\lambda}{\beta \cos \theta}$$

D is the mean (volume average) crystallite size,  $\beta$  is the broadening of its powder diffraction peaks FWHM,  $\theta$  is the usual Bragg angle,  $\lambda$  is the radiation wavelength, and K is a constant which depends on the assumptions made in the theory and often taken as 0.9. We determined the crystallites mean diameter D of the sintered powder from the the XRD peaks after applying the correction for instrumental broadening. Generally,  $\beta$  and D are reciprocally related: the greater the broadening the smaller the crystallite size and vice versa. All the calculated values are tabulated in Table 1. As shown from the table, the highest value of crystallite size is obtained for oxalate method due to high sintering temperature (1000 °C).

### 3.1.2 IR Analysis

Infrared spectra for the  $\text{Ni}_{0.5}\text{Zn}_{0.5}\text{Cr}_{0.1}\text{Fe}_{1.9}\text{O}_4$  were recorded in range 200–1000  $\text{cm}^{-1}$  as shown in Fig. 3 and tabulated in Table 2. The spectra indicate the presence of two absorption bands  $\nu_1$  and  $\nu_2$  as a common feature of all ferrites. The highest one ( $\nu_1$ ) is usually observed in the range 600–549  $\text{cm}^{-1}$  corresponding to intrinsic stretching vibrations of the tetrahedral bond, whereas  $\nu_2$  lowest band is observed in the range 512–406  $\text{cm}^{-1}$  corresponding to stretching vibrations of the octahedral bond [23, 24]. From the table, it is obvious that  $\nu_1$  and  $\nu_2$  are nearly constant for all methods (within experimental error) except  $\nu_1$  for flash with chloride salts and  $\nu_2$  for oxalate, both of them are shifted to higher frequency. Generally, the prediction of increasing frequency for both bands means that, the force constant for such band increases. The increase of force constant is due to decreases of the bond length. This means that the tetrahedral and octahedral bonds are constant for all methods except octahedral bond for oxalate and tetrahedral bond for flash methods, which is in agreement with XRD data. The shift of  $\nu_1$  band for flash (with chloride salt) method can be attributed to decrease of tetrahedral bond due to shortage of  $\text{Zn}^{2+}$  ions that lost during compensation process [25, 26]. This result is mainly due to the high ratio

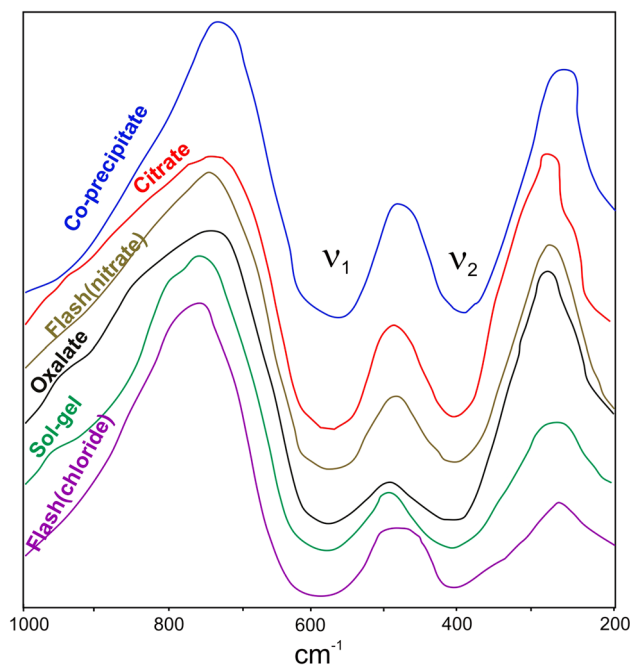


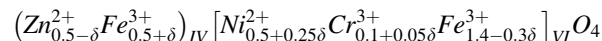
**Fig. 3** IR analysis for  $\text{Ni}_{0.5}\text{Zn}_{0.5}\text{Cr}_{0.1}\text{Fe}_{1.9}\text{O}_4$  prepared by different wet methods

**Table 2** IR bands for  $\text{Ni}_{0.5}\text{Zn}_{0.5}\text{Cr}_{0.1}\text{Fe}_{1.9}\text{O}_4$  nano ferrite prepared by different wet methods

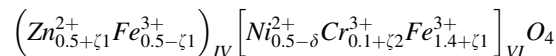
Preparation method	$\nu_1$ ( $\text{cm}^{-1}$ )	$\nu_2$ ( $\text{cm}^{-1}$ )
Co-precipitation	584	408
Flash with nitrate salts	582	410
Sol-gel	583	411
Citrate	582	409
Oxalate	585	416
Flash with chloride salts	596	407

of fuel (urea) with respect to chloride salt. Stoichiometric compositions of metal salts and urea should be calculated based on the components total oxidizing and reducing coefficients for the stoichiometric balance [27]. While, the shift of  $\nu_2$  band for oxalate method can be attributed to decrease of octahedral bond due to shortage of  $\text{Ni}^{2+}$  ions that was lost during precipitation processes this is due to the fact that oxalate ( $\text{C}_2\text{O}_4$ )<sup>2-</sup> is a chelating agent for metal cations. Then, the two methods should be considered as a non stoichiometric systems for the composition  $\text{Ni}_{0.5}\text{Zn}_{0.5}\text{Cr}_{0.1}\text{Fe}_{1.9}\text{O}_4$ . But according to X ray analysis the two systems are single phase of cubic spinel. One attempt to understand this problem [28], is to consider that the non stoichiometric system of the composition  $\text{Ni}_{0.5}\text{Zn}_{0.5}\text{Cr}_{0.1}\text{Fe}_{1.9}\text{O}_4$  can redistribute itself with different cation distribution over the tetrahedral (A) and octahedral (B) sites to

produce a single phase of cubic spinel during synthesis process. So, the system must be normalized to  $\text{A}_1\text{B}_2\text{O}_4$ . Therefore the modified cation distribution for flash method with chloride can be written as:



While for oxalate method is written as:



where  $\delta = \zeta_1 + \zeta_2$  and  $\zeta_1 = 0.93 \delta$ ,  $\zeta_2 = 0.06 \delta$ .

The maximum values of  $\delta$  (the value of loss of metals ions) for both flash (with chloride salt) and oxalate methods are estimated to be 0.36 and 0.13 respectively. The cation distribution for all samples and corresponding parameters are summarized in Table 3. It appears from Table 3 that the values obtained from the above considerations are in agreement with the experimental values.

One can conclude that Ni–Zn–Cr nanoferrite prepared by wet chemical methods display different cation distribution over the tetrahedral (A) and octahedral (B) sites for non stoichiometric systems only. This is due to loss of metals ions during synthesis process.

### 3.1.3 Transmission Electron Microscope (TEM)

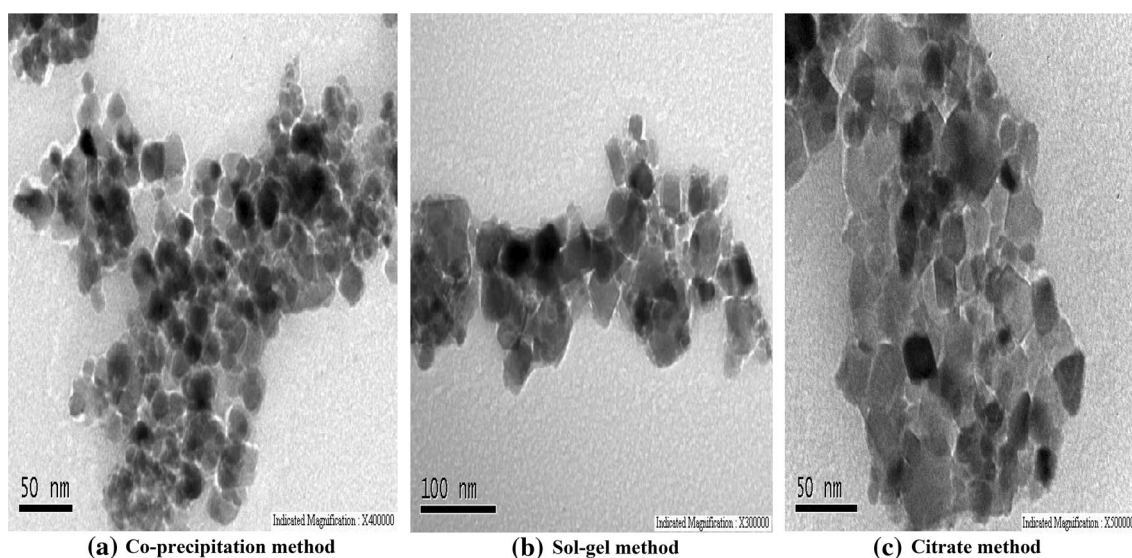
The morphological properties of the nano ferrite powders of  $\text{Ni}_{0.5}\text{Zn}_{0.5}\text{Cr}_{0.1}\text{Fe}_{1.9}\text{O}_4$  prepared by the most three convenient methods (co-precipitation, sol-gel and citrate), are shown in Fig. 4, while the grain sizes data are tabulated in Table 4. It is clear that, the grain size of co-precipitation method is the lowest grain size compared with other methods. TEM images of the investigated samples confirm that, the individual particles are few nanometers in size, which are in good agreement with the calculated grain size by XRD. As shown from Fig. 4 and Table 4, the aggregates size and the shape of the ferrite particles are controlled by the method used. This slight difference in the particle size from XRD and TEM can be explained as the measured size is the result of an average weighed by a six power of the crystal radius because the intensity of XRD is proportional to the square of the volume. Therefore, if the crystals are not perfectly monodisperse, the diffraction signals for bigger diameter are stronger than for the smallest one. As a result, the size measured by XRD should always be smaller than the one covered by electron microscopy. Consequently, the diffraction signals of the largest diameter are stronger than that of the smallest one [29].

### 3.1.4 Atomic Force Microscope (AFM) Analysis

Figure 5 shows the surface morphology of  $\text{Ni}_{0.5}\text{Zn}_{0.5}\text{Cr}_{0.1}\text{Fe}_{1.9}\text{O}_4$  prepared by different wet methods. The figure

**Table 3** Estimated cation distribution, tetrahedral bond, octahedral bond, theoretical lattice parameters and experimental lattice parameters for  $\text{Ni}_{0.5}\text{Zn}_{0.5}\text{Cr}_{0.1}\text{Fe}_{1.9}\text{O}_4$  prepared by different wet methods

Preparation method	Cation distribution	Tetrahedral bond (Å)	Octahedral bond (Å)	$a^{\text{th}}$ (Å)	$a_{\text{exp}}$ (Å)
Coprecipitation	$(\text{Zn}_{0.5}^{2+}\text{Fe}_{0.5}^{3+})_{\text{IV}}$	1.925	2.0348	8.390	8.3891
Flash with nitrate salts	$[\text{Ni}_{0.5}^{2+}\text{Cr}_{0.1}^{3+}\text{Fe}_{1.4}^{3+}]_{\text{VI}}$				8.3879
Sol-gel					8.3840
Citrate					8.3896
Flash with Chloride salts	$(\text{Zn}_{0.15}^{2+}\text{Fe}_{0.85}^{3+})_{\text{IV}}$	1.8854	2.0365	8.3334	8.3347
	$[\text{Ni}_{0.5}^{2+}\text{Cr}_{0.1}^{3+}\text{Fe}_{1.4}^{3+}]_{\text{VI}}$				
Oxalate	$(\text{Zn}_{0.15}^{2+}\text{Fe}_{0.85}^{3+})_{\text{IV}}$	1.93830	2.0313	8.4010	8.4014
	$[\text{Ni}_{0.5}^{2+}\text{Cr}_{0.1}^{3+}\text{Fe}_{1.4}^{3+}]_{\text{VI}}$				

**Fig. 4** TEM image for sample  $\text{Ni}_{0.5}\text{Zn}_{0.5}\text{Cr}_{0.1}\text{Fe}_{1.9}\text{O}_4$  prepared by different wet methods**Table 4** Values of grain size calculated from XRD and from TEM for  $\text{Ni}_{0.5}\text{Zn}_{0.5}\text{Cr}_{0.1}\text{Fe}_{1.9}\text{O}_4$  prepared by different wet methods

Preparation method	Grain size calculated from	
	XRD (nm)	TEM (nm)
Co-precipitation	16.4	26
Sol-gel	22.6	30
Citrate	33.8	35

demonstrates that, the grain size and the surface roughness for different samples have various values, indicating that, the preparation method has prime role controlling the properties of the synthesized ferrite. Figure 6 shows the particles sizes distribution which is used to determine the agglomeration of particles in the samples. From the figure,

it is noticed that the citrate and co-precipitation methods have narrow size distribution. The broad particles sizes distribution for flash method is probably due to the occurrence of local combustion. Figure 6 shows that the mean particle sizes are in agreement with those obtained from XRD and TEM analyses.

### 3.2 Magnetic Properties

Room temperature magnetization for nanocrystalline  $\text{Ni}_{0.5}\text{Zn}_{0.5}\text{Cr}_{0.1}\text{Fe}_{1.9}\text{O}_4$  prepared by different wet methods, is shown in Fig. 7 and all data are tabulated in Table 5. As shown from the figure, the hysteresis loop shows a normal (s-shape) type of ferrimagnetic behavior, the size and the shape of the hysteresis curve for a magnetic material are of considerable practical importance. The relative thin and narrow area of the loop is related to the specific behavior for soft ferrite (easy magnetization and demagnetization).

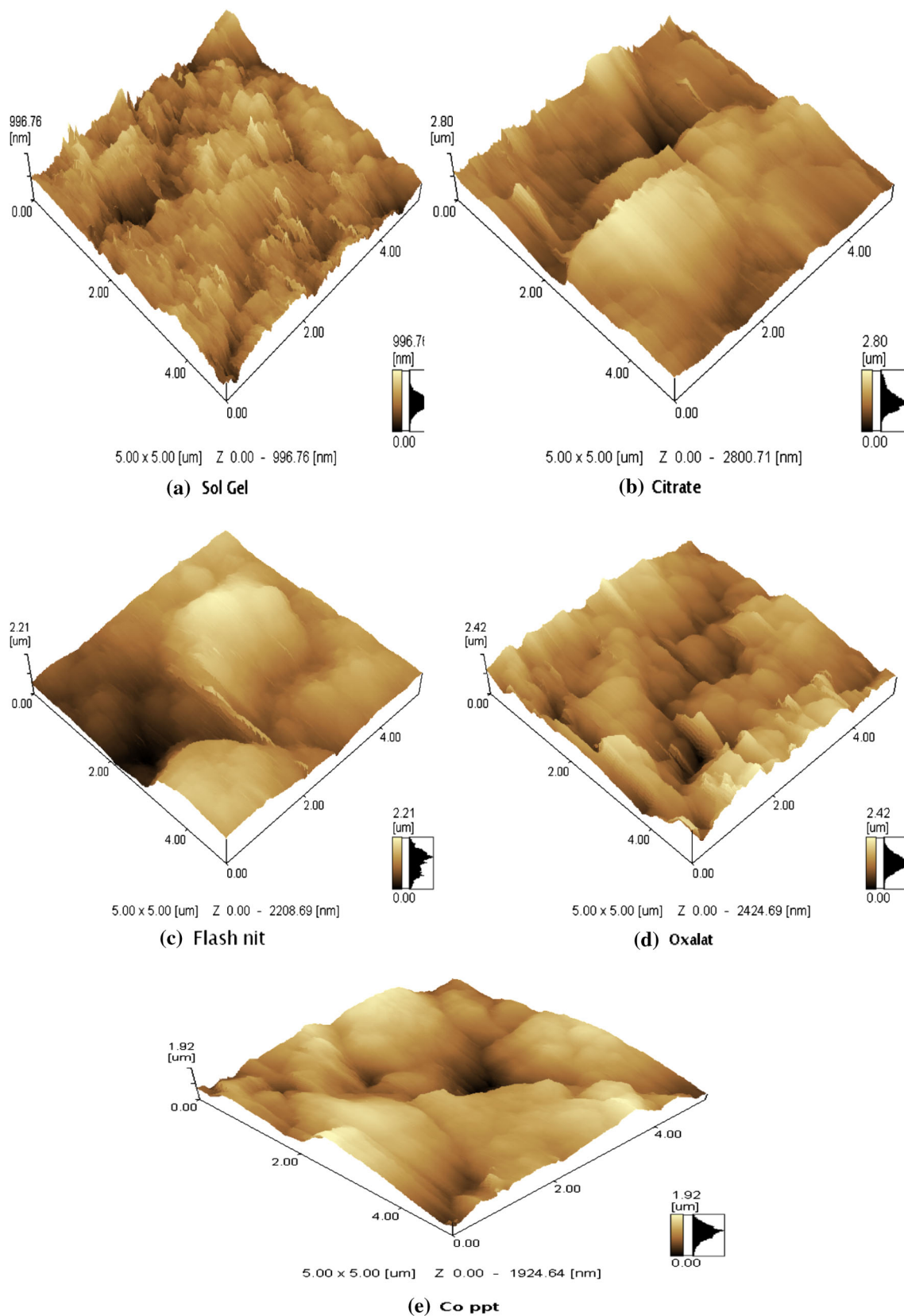


**Fig. 5** 3D atomic force microscopy images for  $\text{Ni}_{0.5}\text{Zn}_{0.5}\text{Cr}_{0.1}\text{Fe}_{1.9}\text{O}_4$  prepared by different wet methods

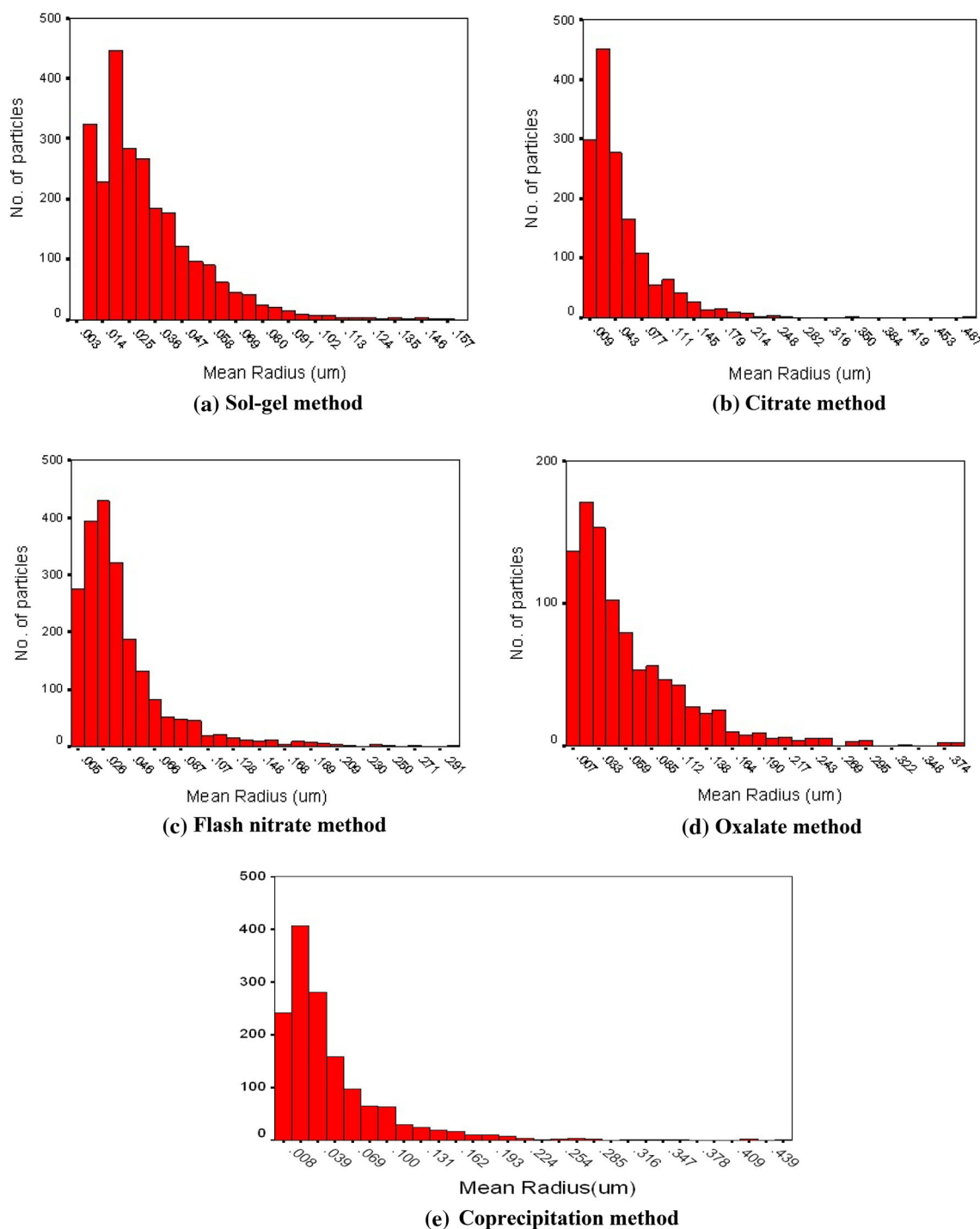


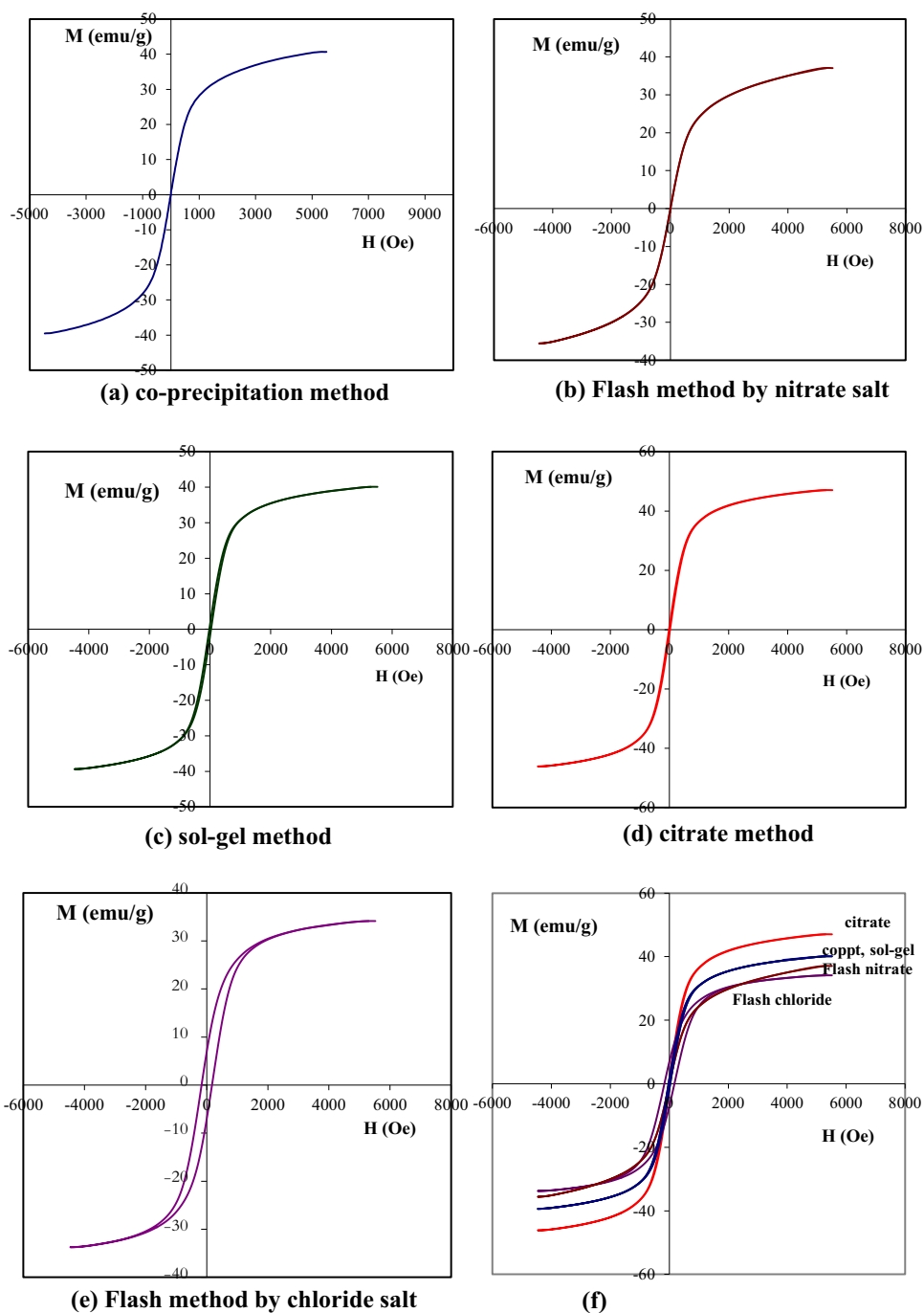
**Fig. 6** Grain size distribution diagrams for  $\text{Ni}_{0.5}\text{Zn}_{0.5}\text{Cr}_{0.1}\text{Fe}_{1.9}\text{O}_4$  prepared by different wet methods

Generally, energy dissipated per unit volume in each cycle, is proportional to the area enclosed by the hysteresis loop. It is desirable that the hysteresis loop of the investigated samples should be narrow to minimize losses, as in our cases. According to Néel’s molecular field model [30], the A-B super exchange interaction predominates the intra sub lattice A–A and B–B interaction. Therefore, the net

magnetic moment is given by the sum of the magnetic moments of the A and B sub lattices. It is clear from the figure that, the saturation magnetization of nanosamples prepared by flash (with chloride salts) method is the lowest one while the citrate and co-precipitation methods have the highest  $M_s$ . This result confirms the hypothesis of shortage of  $\text{Zn}^{2+}$  ions that were lost during compensation processes.



**Fig. 7** Magnetic hysteresis loops for  $\text{Ni}_{0.5}\text{Zn}_{0.5}\text{Cr}_{0.1}\text{Fe}_{1.9}\text{O}_4$  prepared by different wet methods



So the decrease of  $\text{Zn}^{2+}$  increases the magnetic moment in sublattice A which will decrease the net overall magnetic moment in the lattice. While the observed higher values of saturation magnetization (citrate, co-precipitation and sol-gel), can be explained on the basis of grain size and the exchange interaction among the adjacent nano-grains. The exchange interaction leads to intergranular magnetic correlations in the investigated samples with density packed grains [31]. The squareness ratio is given by the ratio of

$(M_r/M_s)$  and is essentially a measure of how square the hysteresis loop is. In general large SQR values are desired for recording medium [32]. While Magnetic anisotropy is an intrinsic property describing magnetic materials and is related to the arrangement of atoms in the crystal lattice. This property originates from spin-orbit interactions [33]. All the calculated and measured parameters are tabulated in Table 5. As shown from Table 5, most of the investigated nanosamples exhibit high saturation magnetization values

**Table 5** Coercive field ( $H_c$ ), saturation magnetization ( $M_s$ ), remanent magnetization ( $M_r$ ), squareness and anisotropy constant for  $Ni_{0.5}Zn_{0.5}Cr_{0.1}Fe_{1.9}O_4$  nanoferrite prepared by different wet methods

Method of preparation	$H_c$ (Oe)	$M_s$ (emu/g)	$M_r$ (emulg)	Squareness ( $M_r/M_s$ )	Anisotropy constant (Oe emu/g)
Coprecipitation	16.45	40.74	4.602	0.113	683.85
Flash with nitrate salts	35.33	37.02	3.930	0.106	1334.61
Sol-gel	28.15	40.30	7.290	0.181	1157.60
Citrate	15.02	47.26	8.371	0.177	724.33
Flash with chloride salts	182.20	34.36	8.441	0.246	6388.16

and small coercive fields. The saturation magnetization, in general has been noticed in the range of 40–110 emu/g for bulk ferrite materials [34], whereas for nanoferrites it is shown to vary from 10 to 70 emu/g [35].

From a closer look to the Table 5, and the Fig. 6a–e, one can find that, the coercivity has a general trend with particle size distribution where the citrate and co-precipitation methods show the minimum values of coercivity. While there is a relation between  $M_s$  and  $H_c$  in which  $H_c$  has an inverse trend with  $M_s$ , i.e., the highest  $M_s$  has the lowest  $H_c$  and vice versa [36]. The large value of  $H_c$  can be explained in view of dependence of it on the effective anisotropy of the particles according to the Stoner–Wolfarth model [37]. The effective anisotropy of the particles is the sum of the contributions of magnetocrystalline anisotropy and shape anisotropy. Therefore, increases the effective anisotropy is due to its large aspect ratio, which results in a high  $H_c$  as reported by Guohong et al. [38]. For oxalate method A large value of  $H_c$  is attributed to the increase of the average particle size This can be understood by the fact that as the domain contains many grains, the magnetocrystalline anisotropy is averaged over many grains and various orientation. The large anisotropy leads to a increase in coercivity with increasing grain sizes [39].

Finally, the previous discussion shows that the properties such as particle size and magnetic properties of NiZnCr nanoferrite processed by citrate and co-precipitation methods are comparable to and in some cases even better than those reported for nanoferrite prepared by other wet methods.

## 4 Conclusions

- (1) Ni–Zn–Cr nanoferrite prepared by wet chemical methods display different cation distribution over the tetrahedral (A) and octahedral (B) sites for non stoichiometric systems only.
- (2) For any wet-chemical method, one have to check whether the prepared samples retain the stoichiometric composition using atomic absorption spectroscopy (metal ion analysis).

- (3) The value of lattice parameter is very good indicator that plays a significant role in determining the stoichiometric cation distribution of the composition.
- (4) The citrate and co-precipitation methods are the effective in providing smallest average crystallite size. It is remarkable to achieve highest value of saturation magnetization. Also, both require neither expensive precursors nor environment unfriendly solvent, nor extremely higher pressure.

## References

1. K.H. Lee, D.H. Cho, S.S. Jeung, J. Mater. Sci. Lett. **16**, 83 (1997)
2. A. Verma, T.C. Goel, R.G. Mendiratta, M.I. Alam, Mater. Sci. Eng. B **60**, 156 (1999)
3. P. Srinivasu, K. Suresh, G. Datt, A.C. Abhayankar, P.N. Rao, M.L. Kantam, S.K. Bhargava, J. Tang, Y. Yamauchi, Phys. Chem. Chem. Phys. **16**, 22471 (2014)
4. M.B. Zakaria, A.A. Belik, C.H. Liu, H.Y. Hsieh, Y.T. Liao, V. Malgras, Y. Yamauchi, K.C. Wu, Chem Asian J. (2015) doi:10.1002/asia.201500232
5. B.P. Bastakoti, H. Sukegawa, K.C.-W. Wu, Y. Yamauchi, RSC Adv. **4**, 9986 (2014)
6. J. Smith, H.P.J. Wijn, *Les Ferrites* (Bibliography Tech Philips, Paris, 1961)
7. A. Verma, T.C. Goel, R.G. Mendiratta, P. Kishan, J. Magn. Mater. **208**(1–2), 13 (2000)
8. P.J. van der Zaag, A. Noordermeer, M.T. Johnson, P.F. Bongers, Phys. Rev. Lett. **68**(20), 3112 (1992)
9. A.R. Corradi, L. Benzoni, C.A. Nannetti, M. Petrer, S.S. Pizzini, J. Phys. Colloq. **38**, C1-291 (1977)
10. M. Petrer, A. Gennaro, N. Burriesci, J. Mater. Sci. **17**, 429 (1982)
11. H. Yasuoka, A. Hirai, T. Shinjo, M. Kiyama, Y. Bando, T. Takada, J. Phys. Soc. Jpn. **22**, 174 (1967)
12. A.M. Kumar, M.C. Varma, C.L. Dube, K.H. Rao, C. Kashyap, J. Magn. Mater. **320**, 1995 (2008)
13. B.D. Cullity, S.R. Stock, *Elements of X-ray diffraction*, 3rd edn. (Prentice-Hall Inc., New Jersey, 2001), p. 388
14. B. Gillot, D. Thiebaut, D. Thiebaut, M. Laarj, Thermochem. Acta **342**, 167 (1999)
15. K.E. Sickafus, J.M. Wills, N.W. Grimes, J. Am. Ceram. Soc. **82**(12), 3279 (1999)
16. R.J. Hill, J.R. Craig, G.V. Gibbs, Phys. Chem. Miner. **4**, 317 (1979)
17. Periodic Table SARGENT-WELCH Scientific Company 7300 Linder Avenue Skokie Illinois 60076 Catalog Number 5-18806.

- <http://www.sargentwelch.com/store/catalog/searchCategory.jsp?id=PD10367142&searchUrl=/s>
18. G Blasse, Philips Res. Rep. Suppl., **3**, 1 (1964)
  19. D.S. McClure, J. Phys. Chem. Solid **3**, 311 (1957)
  20. R. Valenzuela, *Magnetic Ceramics* (University press, Cambridge, 1994)
  21. J.M. Dunitz, L.E. Orgel, J. Phys. Chem. Solid **3**, 381 (1957)
  22. R.D. Shannon, Acta Crystallogr. **A32**, 751 (1976)
  23. R.D. Waldron, Phys. Rev. **99**(6), 1727 (1955)
  24. W.B. White, B.A. De, Angel. Spectrochim. Acta **A23**, 985 (1967)
  25. P.I. Slick, in: *Ferrites*, ed. by Y. Hoshino, S. Lida, M. Sugimoto. Proceedings of the International Conference, Japan, July 1970, (University Park Press, Baltimore, 1971), p.81
  26. P. Sainamthip, R.W. Amarakoon, J. Am. Ceram. Soc. **71**(8), 644 (1988)
  27. M. Rajendran, R.C. Pullar, J. Magn. Magn. Mater. **232**(1–2), 71 (2001)
  28. L.M. Salah, Phys. Stat. Sol. A **203**(2), 2006 (2006)
  29. P. Mathura, A. Thakura, M. Singha, J. Magn. Magn. Mater. **320**, 1364 (2008)
  30. L. Néel, Ann. Phys. **3**, 137 (1948)
  31. L.G. Loffler, H.B. Brajin, W. Wagner, Phys. Rev. Lett. **85**, 1990 (2000)
  32. S.C. Goha, C.H. Chiaa, S. Zakariaa, M. Yusoffa, C.Y. Hawa, S.H. Ahmadia, N.M. Huangb, H.N. Limc, Mater. Chem. Phys., **120**, 31 (2010)
  33. L.M. Salah, M.M. Rashad, M. Haroun, M. Rasly, M.A. Soliman, J. Mater. Sci. **26**, 2015 (1045)
  34. S.L. Pereira, H.D. Pfannes, A.A.M. Filho, Mater. Res. **2**(3), 231 (1999)
  35. A.S. Albuquerque, J.D. Ardisson, W.A.A. Macedo, J. Appl. Phys. **87**(9), 4352 (2000)
  36. M.H. Han, Georgia Institute of Technology, 98 (2008). <https://smartech.gatech.edu/handle/1853/26465?show=full>
  37. E.C. Stoner, E.P. Wohlfarth, Phil. Trans. Roy. Soc., **A240**, 599 (1948) Reprinted in IEEE Trans. Magn., **27**, 3475 (1991)
  38. G. Mu, X. Pan, N. Chenand, K. Gan, Mater. Res. Bull. **43**, 1369 (2008)
  39. Z. Zi, H. Lei, X. Zhu, B. Wang, S. Zhang, X. Zhu, W. Song, Y. Sun, Mater. Sci. Eng. B **167**, 70 (2010)